

# Testing Vascular Modelling Principles by Generating Virtual Vascular Networks

Panagiotis Lymperopoulos, Alexander Brummer, Van M. Savage

June 1, 2019

## 1 Abstract

Successful modelling of vascular structure can both further our understanding of metabolism in multicellular organisms and lead to the development of effective diagnostic tools for vascular disease. Testing the fundamental assumptions of vascular modelling is a crucial step toward realizing those aims. Here I evaluate whether space filling, minimal resistance to fluid transport and minimal building cost are valid and sufficient principles to build realistic vascular structure. I generate virtual vascular networks based on these principles, examine their impact on network structure and use the West-Brown-Enquist framework to describe their scaling properties. I then compare the scaling properties of virtual networks with those of mammalian and plant networks and observe that the combination of space-filling, minimization of resistance to fluid transport and minimization of building cost predict high asymmetry in sibling vessel radii. The largely symmetric branching of mammalian vasculature and the mix of symmetry and asymmetry in plant vascular structure support that at least one crucial component that favors network symmetry over asymmetry is absent from the model. Additionally, I find that some assumptions have equivalent effects on network structure despite constraining different geometric features of vessels. Future work can extend our network generator and utilize our insights to understand and describe the missing components to formulate a more complete picture of the forces governing vascular structure.

## 2 Introduction

Vascular systems are among the most pervasive resource distribution networks found in nature. They are tasked with delivering resources across various organs and systems, perhaps most importantly those associated with an organism’s metabolism. Resource exchange between the vascular system and surrounding tissues happens on the capillary level through diffusion across cell membranes. Although not strictly the case, it is commonly assumed that capillary characteristics remain the same across organisms of various scales [1] and so allow us to make consistent comparisons of

resource distribution among different organisms. This commonality, along with the crucial role of the capillary bed in the metabolic process, led West, Brown and Enquist to develop a general theory (WBE) that attributes the observed  $B \approx M^{3/4}$ [2] relationship of metabolic rate (B) and mass (M) to the self-similar space-filling nature of the vascular system and other resource distribution networks [3, 4, 5].

WBE-theory and its more generalized variants [6] provide more than just an explanation of the metabolic rate and mass relationship. They also develop a mathematical framework to describe vascular structures and quantify their properties. Therefore, the success of the theory not only advances our understanding of biological processes but may also lead to clinical applications. Recent advances in vascular imaging [7] along with the WBE framework can facilitate applications such as tumor detection due to localized abnormal vascular growth. In recent yet unpublished work, members of the Savage Lab utilize the mathematical framework of WBE to distinguish between mammalian and plant networks and ongoing work aims to expand the framework to include more aspects of vascular structure. Such applications depend on the ability of WBE to accurately describe vascular networks, which in turn relies on the validity of the theory's assumptions about network structure [8].

Previous work has attempted to generate virtual vascular networks by simulating vessel length, in order to examine asymmetry in space-filling networks [9]. Others have simulated vascular growth around tumors to observe large-scale network properties [10]. The present work aims to examine whether WBE's assumptions about vascular network structure are valid and sufficient to generate realistic vascular structure. This is achieved by generating virtual vascular networks (VVNs) that follow theoretically inspired constraints and comparing them to real networks using WBE's analytical framework. Additionally, the simulation developed allows us to make an assessment of the competing factors that determine vascular structure by varying their influence on network growth and observing the resulting network properties.

The constraints used to generate VVNs are expressions of WBE's assumptions that vascular

networks are space-filling and that the evolutionary process will have minimized both power loss due to blood flow and material building cost. The space-filling constraint is addressed by forcing the generated networks to deliver blood on a predetermined set of points that represent vessel service areas. The points are placed as in the work by Hunt and Savage [9] so that no two points are closer than one service-area radius. Delivering resources to one of these points is sufficient to supply the surrounding area, as is the case with capillary vessels that rely on diffusion to serve a volume of cells around them. In this work, we assume that power loss occurs primarily through impedance to blood flow[8]. A global metric of effective network-wide impedance is measured, as well as a local metric for every vessel branching junction. Measures of building cost follow previous work[9] in considering overall network efficiency and total network length.

## 3 Materials and Methods

### 3.1 Virtual Vascular Network Generator

The simulation developed optimizes a population of VVNs by minimizing combinations of metrics that reflect power loss due to blood flow and material building cost. The VVNs are trees that span a predetermined grid of points that fills a disk. Each point represents the center of the service area of each vessel and each edge of the tree represents a single vessel. A VVN delivers blood to a point by creating an edge between that point and either the heart or another point already supplied with blood. Network optimization occurs via a genetic algorithm, which involves encoding networks into “genes” and applying a selection pressure for networks that adhere to WBE’s assumptions.

#### 3.1.1 Network encoding

In order to carry out the optimization via genetic algorithm, VVNs need to be encoded in one dimensional data structures. A VVN’s genetic code is made up of two strings of numbers, each encoding a different aspect of vascular tissue. The first string represents the “structural gene”, that is the gene that encodes information about the network structure, while the other represents the “radius gene” which encodes a radius value for every vessel.

The structural gene encoding method, inspired by the work of Palmer and Keshenbraum [11], translates a gene consisting of a string of binary numbers into a tree. Each number in the string represents the weight of an edge in a fully connected graph of size equal to the number of service volumes in the network plus one to account for the heart. A decoding procedure based on a modified version of Prim’s algorithm, constructs a minimum spanning tree from the set of weights and that tree determines the structure of the vascular network. This encoding scheme is able to represent every possible spanning tree of a graph, which allows for all possible structures of a vascular network to be searched. Additionally, the use of a modified Prim’s algorithm, limits the search space to trees only, thus avoiding the computational overhead of repairing broken genes that fail to represent a

tree.

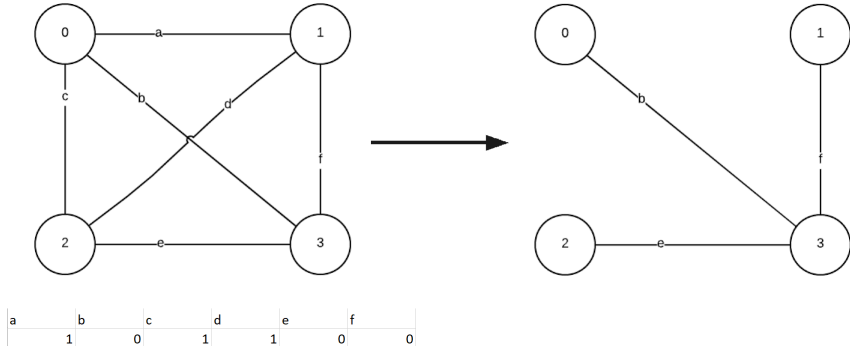


Figure 1: **Encoding of a 4 point tree structure into a gene.** The table on the bottom left is the gene corresponding to the resulting tree (right). It specifies a weight for every edge a-f of the complete graph (left). The encoded tree is the MST of the complete graph.

The radius gene is a collection of real numbers ranging from a minimum capillary radius to a maximum “heart” radius that signifies the maximum radius possible for a given run of the simulation. The  $i_{th}$  entry of the radius gene corresponds to the radius of the vessel delivering blood to the  $i_{th}$  service volume. The two genes together define a single network that is evaluated based on measures of its material building cost and power-loss due to blood flow.

### 3.1.2 Measures of Network Optimality

Network optimality in the context of the present work corresponds to a network’s adherence to WBE’s assumptions. All networks fulfill the space filling assumption due to the spacial distribution of the points which they span. Power loss minimization and building cost minimization are expressed as functions of network properties and combined into a cost function that must be minimized. Therefore, a network is deemed optimal when its cost function reaches a global minimum, but due to the complexity of the problem only sub-optimal solutions can be reached in reasonable time.

In Hunt and Savage [9], the material building cost of a network is assumed to be related to its total path length, meaning the sum of the lengths of all vessels in the network. They also consider

the mean path length of a network as a measure of network efficiency related to the time it takes for resources to be delivered to every cell. Both of these metrics are included in our work and are computed as follows.

$$Total\ Path\ Length = \sum_{i=0}^n length_i \ for\ i \in Vessels \quad (1)$$

$$Mean\ Path\ Length = Total\ Path\ Length / Number\ of\ paths \quad (2)$$

Power loss occurs due to impedance to blood flow. Regardless of the source of the impedance, the effective impedance of an entire network can be calculated using principles from electrical circuits in physics. Vessels that originate from the same branching point are treated as connected in parallel and vessels along the same chain are treated connected in series. In this work, the dissipation cost of a network is defined as its effective impedance and is a metric of power loss due to energy dissipation. For a given network, dissipation cost is calculated using the following formulas, where  $z_i$  represents the impedance of a single vessel and is a function of its geometric properties.

$$Dissipation\ Cost = \begin{cases} \sum_{i \text{ chain}} z_i & \text{for vessels in series} \\ \frac{1}{\sum_{i \text{ sibling vessels}} \frac{1}{z_i}} & \text{for vessels in parallel} \end{cases} \quad (3)$$

Whereas dissipation cost is a global network metric for impedance to blood flow, we also consider impedance constraints on the level of branching junctions. During pulsatile flow, in real vascular tissue seen mostly in larger vessels, impedance is primarily due to wave reflections. As blood travels down the vessel in waves and reaches a branching junction, the waves are reflected on the vessel walls and interfere with the next incoming wave. These reflections can be eliminated through impedance matching which for the purposes of this work reduces to preserving cross-sectional area across branching junctions. Deviation from the impedance matching regime is penalized in our

algorithm and is computed as follows.

$$\text{Wave Reflection Cost} = \sum_p \{radius_p^2 - \sum_c radius_c^2\} \quad (4)$$

Here,  $radius_p$  and  $radius_c$  are the radii of the parent and children vessels at a single branching point. For every branching junction, the difference between the cross sectional area of the parent and the sum of cross sectional areas of all child vessels contributes to the network cost function.

These metrics are combined in a single fitness function and their importance in the optimization and thus impact on network structure are tuned using a weighting coefficient. The cost function is a linear combination of the various costs. The fitness of a network, which determines its probability of producing offspring, is defined as the inverse of the total cost.

$$\text{Total Cost} = \alpha_1 * \text{Total Path Length} + \alpha_2 * \text{Mean Path Length} \quad (5)$$

$$+ \alpha_3 * \text{Dissipation Cost} + \alpha_4 * \text{Wave Reflection Cost}$$

$$\text{Fitness} = 1/\text{Total Cost} \quad (6)$$

### 3.1.3 Genetic Operators

For the optimization process to proceed we use two genetic operators that modify genes in one generation to produce offspring that populate the next generation. Crossover is the operator responsible for combining the genes of two networks to produce two novel network structures that share their parents' characteristics. The combination of genes is achieved by replacing segments of one parent's genes with corresponding segments from the other parent. The result is a pair of individuals sharing complementary segments of their parent's genetic material. The success of crossover at producing individuals of higher fitness depends on the method of selecting parents to produce the next generation, and on maintaining genetic diversity in the population so that the algorithm avoids premature convergence.

Tournament selection [12] is used to select parents as it ensures that higher-fitness individuals are selected while maintaining genetic diversity. Nevertheless, after a few generations all individuals

end up being closely related and as a result a drop in genetic diversity is unavoidable. A mutation operator is used to introduce further genetic diversity to the population. Higher genetic diversity means that it is more likely that at least one individual will develop an innovation that will result in an increase in fitness. The operator is governed by a mutation rate parameter  $\mu$  that is the probability of making a random change to an individual's genetic code. The value of the mutation rate parameter was subject to experimentation as it depends on population size, the particular gene encoding scheme and the problem formulation.

### 3.2 Network Comparison and Data

In order to consistently compare the virtual networks with each other and with real world vascular networks, we use the WBE framework to quantify their scaling properties [3].

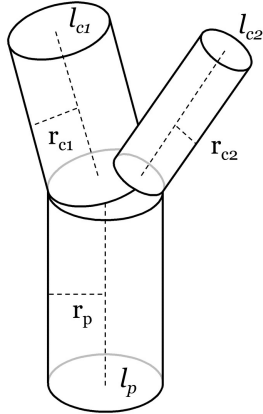


**Figure 2: Parameterization of a vessel branching junction.**  $r_p$  and  $l_p$  denote the radius and length of the parent vessel and  $r_{ci}$  and  $l_{ci}$  denote the radius and length of the  $i$ th child vessel.

In this work we focus on the scaling of vessel lengths and radii across networks. We quantify

network scaling by measuring the following scale factors for all parent-child pairs of vessels.

$$\beta = r_c/r_p \quad (7)$$

$$\gamma = l_c/l_p \quad (8)$$

By measuring the scale factors for a group of related networks we obtain distributions which we compare using a Welch's t-test. Various settings of our VVN generator are used to produce different network structures which are then compared to each other and to a data set of mammal and plant networks.

The data set, first used by Brummer et al in work recently submitted for publication [13], consists of a variety of mammal and plant networks from various species. Specifically, the mammal data set consists of major arteries of the adult human head and torso of 18 individuals (*H. sapiens*) and one complete vascular network from a mouse lung (*M. musculus*). The plant networks consist of canopy terminal ends of Maple (*A. grandidentatum*), Scrub Oak (*Q. gambelii*), Robinia (*R. neomexicana*), White Fir (*A. concolor*), Douglas Fir (*P. menziesii*), and White Pine (*P. strobiformis*). It also includes one adult tree (excluding roots) from the species Balsa (*O. pyramidale*), one Pinon (*P. edulis*) and five Ponderosa pines (*P. ponderosa*). Finally, the plant networks also include root clusters from Andean tropical montane cloud forests. Previous work indicates that scaling relationships of tree xylem follows those of the external body of the tree [14, 15] which justifies our use of external measurements as proxies for internal vascular structure. Since not enough data is available to draw species-specific conclusions, we group the data into mammal and plant networks to observe general trends.

## 4 Results

In this section we present the results obtained by the various components of the project. First we provide evidence of the efficacy of the VVN generator, then we present limits of convergence for individual metrics and for certain combinations and finally we compare the generated VVNs with our mammal and plant data.

### 4.1 VVN Generator

The VVN generator is able to optimize a population of VVNs for any combination of the aforementioned metrics. The size of the generated population can be tuned depending on the computational power of the device running the generator, with more powerful computers being able to optimize larger populations and so decreasing the time to convergence. For a fixed population size of 200 individuals, various mutation rate values where tested.

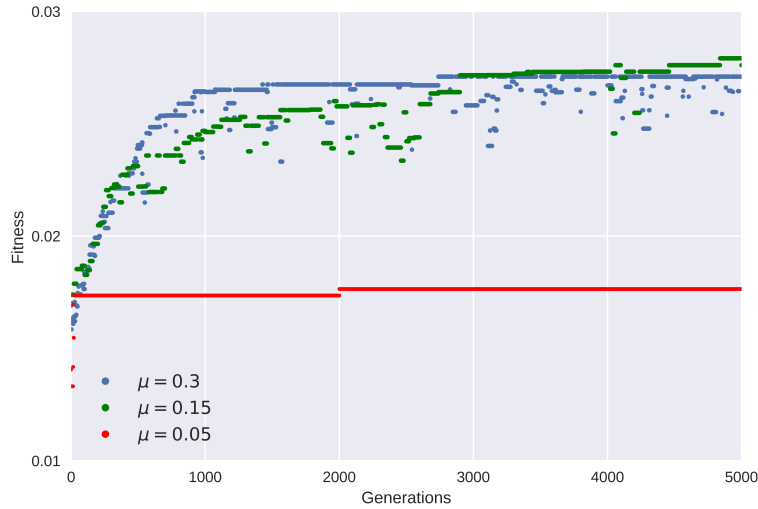
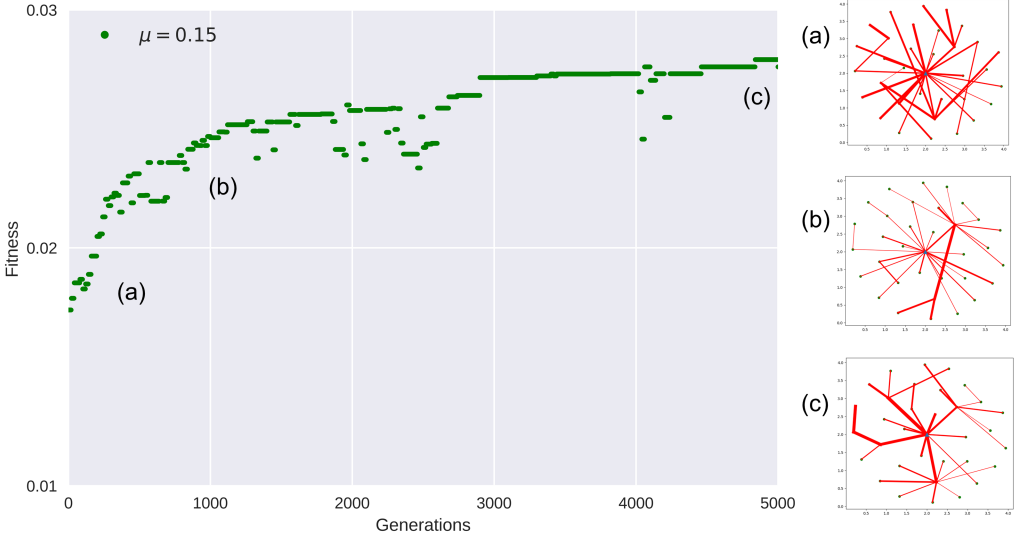


Figure 3: **Fitness graph for different mutation rates.** The red line indicates the fitness of a randomly selected individual over 5000 generations when the probability of mutation for each gene is 0.05 ( $\mu = 0.05$ ). The green line corresponds to a probability of mutation of 0.15 ( $\mu = 0.15$ ) and the blue line to a probability of 0.3 ( $\mu = 0.3$ ).

A mutation rate that is very small makes it so the population of networks quickly converges to a sub-optimal solution (Fig.3). The reason being that after a few generations all individuals are closely related and so new network structures are sampled very infrequently. A very high mutation rate achieves a sharp increase in fitness in the beginning, but tends to level off in a sub-optimal solution. We argue that for individuals that achieve higher fitness, a random change in their genetic code is more likely to be deleterious than beneficial and as a result, as the average population fitness increases, frequent mutations become destructive to an overall fit population. An intermediate mutation rate, although initially yielding a slower increase in fitness, is beneficial in the long term as it achieves a balance between high genetic diversity and prevalence of useful features.



**Figure 4: Evolution of a VVN for building cost and power loss.** Initially networks are completely random. As the algorithm proceeds, network connectivity starts becoming more efficient and the overall volume of the network rapidly decreases. The following generations refine network structure and radii until the algorithm converges near a local minimum.

Once all parameters for optimization are set, a population of random networks is generated. Initially genetic diversity is very high and the population is far away from a near-optimal solution, so fitness increases very rapidly. As the population starts becoming more uniform and approaches a sensible solution, the optimization starts to level off and only small improvements are made to the networks. Given enough time, the population converges to a local minimum of the cost function.

## 4.2 Limits of Network Optimality

In this section we present the network structures expected by optimizing for each of our criteria and the network characteristics produced by optimizing for pairwise combinations of them. These limits of optimality inform our intuition for understanding the network structures produced by further

combinations of optimization criteria.

#### 4.2.1 Single Criterion Optimization

The following network structures and properties are theoretical results that we expect to observe in networks that optimize for one criterion at a time.

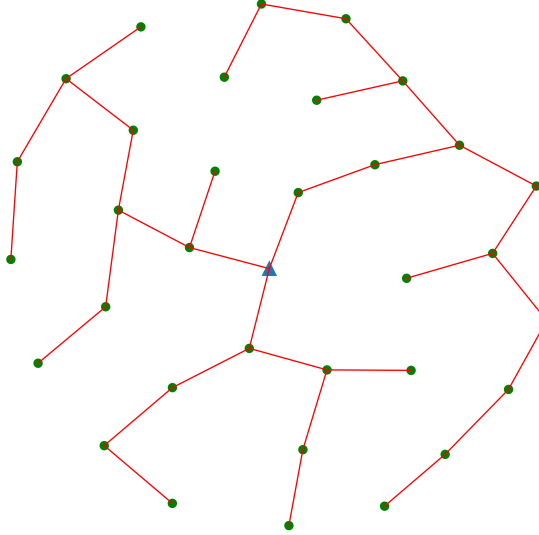


**Figure 5: Network Optimized for Total Path Length** Optimization for total path length is akin to finding the minimum spanning tree of the heart and service areas. The resulting tree is only dependent on the geometry of the service areas and does not favor any particular branching characteristics. Vessel radii are set to a uniform value since they have no influence on total path length.

Total path length, being a metric of network building cost, should be optimized by network structures whose vessels are as short as possible. This problem maps naturally into finding the minimum spanning tree of a weighted graph, where a weight is the distance between two points and the graph is the complete graph connecting every point (service area or the heart) to every other one. A network optimized for total path length alone should approximate the minimum spanning tree of its points, while a network that has total path length as only one of its optimization criteria,

should sometimes sacrifice building cost in favor of other features.

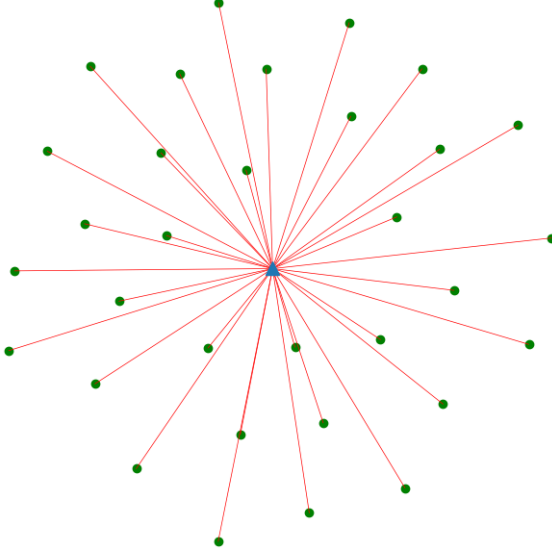


**Figure 6: Network Optimized for Dissipation or Mean Path Length** Optimization for dissipation alone results in star-burst network structures with small vessel radii. Mean path length also favors star-burst structures but exerts no selection pressure on vessel radii.

As outlined earlier, the calculation of energy dissipation originates in the modeling of vascular networks as circuits of resistors. As a result, optimizing for energy dissipation favors highly parallel connectivity, as the effective impedance (or in the case of electrical circuits the effective resistance) of the network is minimal when all sources of impedance are connected in parallel. The network structures that achieve this highly parallel architecture are those that connect every service area directly to the heart. Since vessel radii are also undergoing selection pressure when optimizing for dissipation and the impedance of a vessel depends in part on its radius, all radii values tend to converge to the minimum value allowed in the model.

The strategy of connecting all vessels in parallel is also the one favored by mean path length. Since a path is defined as a sequence of vessels from the heart to a terminal point (i.e. a point on which no further branching occurs), minimizing mean path length is achieved by connecting every point directly to the heart, thus maximizing the number of paths in the network. Although

originally mean path length is meant to be a proxy for efficient resource delivery, it seems that in our model, this effect can be achieved as a byproduct of minimizing energy loss due to dissipation in the network. Finally, much like total path length, mean path length exerts no selection pressure on vessel radii.

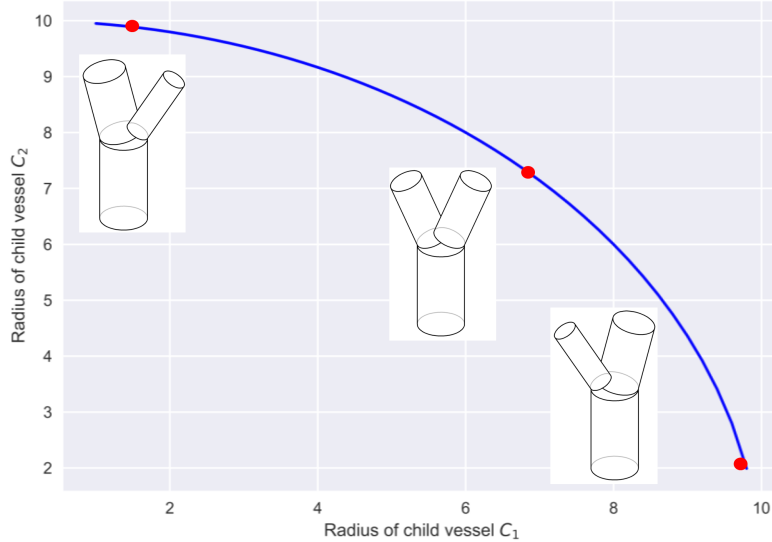


**Figure 7: Impedance matching does not favor symmetric or asymmetric branching.** Wave reflections are eliminated by impedance matching. The blue line indicates the range of child radii values that achieve impedance matching when the parent vessel has a radius of 10 units.

Wave reflections occur when there is a mismatch of vessel cross-sectional area across a branching junction [8]. Figure 7 shows the region of values of child vessel radii where the total cross sectional area of child vessels equals that of the parent vessel, thus achieving impedance matching. In this region, wave reflections in the branching junction are eliminated. As indicated in Figure 7, impedance matching can occur both in symmetric and asymmetric branching points. Therefore, a network optimized for minimizing wave reflections should exhibit a mix of symmetric and asymmetric branching.

#### 4.2.2 Optimization Criteria Interactions

In this section we examine some pairwise interactions of optimization criteria. Although more combinations are possible than the ones shown here, we have limited the discussion to those that produce biologically meaningful results.

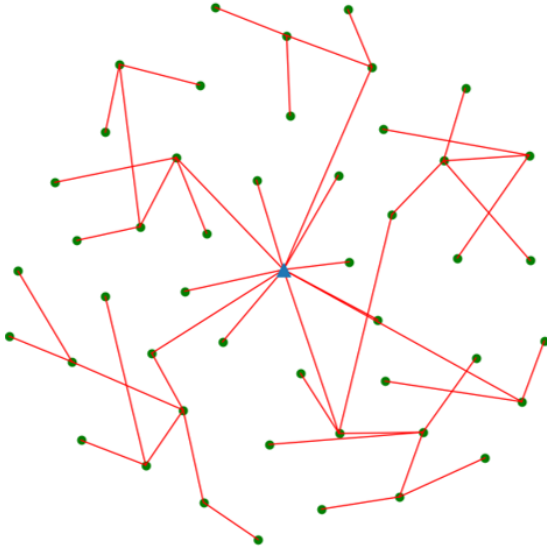


Figure 8: **Network optimized for total path length and dissipation cost (or mean path length).** The tendency of dissipation and mean path length to generate highly parallel networks is mitigated by the tendency to minimize material building cost.

Optimizing networks for the combination of total path length and mean path length produces networks that exhibit a balance between material cost and resource delivery efficiency. Optimizing for energy loss due to dissipation along with total path length has a similar effect on network structure, with the only difference being that radii values converge to the minimum value allowed. The amount of branching observed in these networks depends on the relative weights of the two metrics, as increased branching is heavily favored by the dissipation and mean path length metrics.

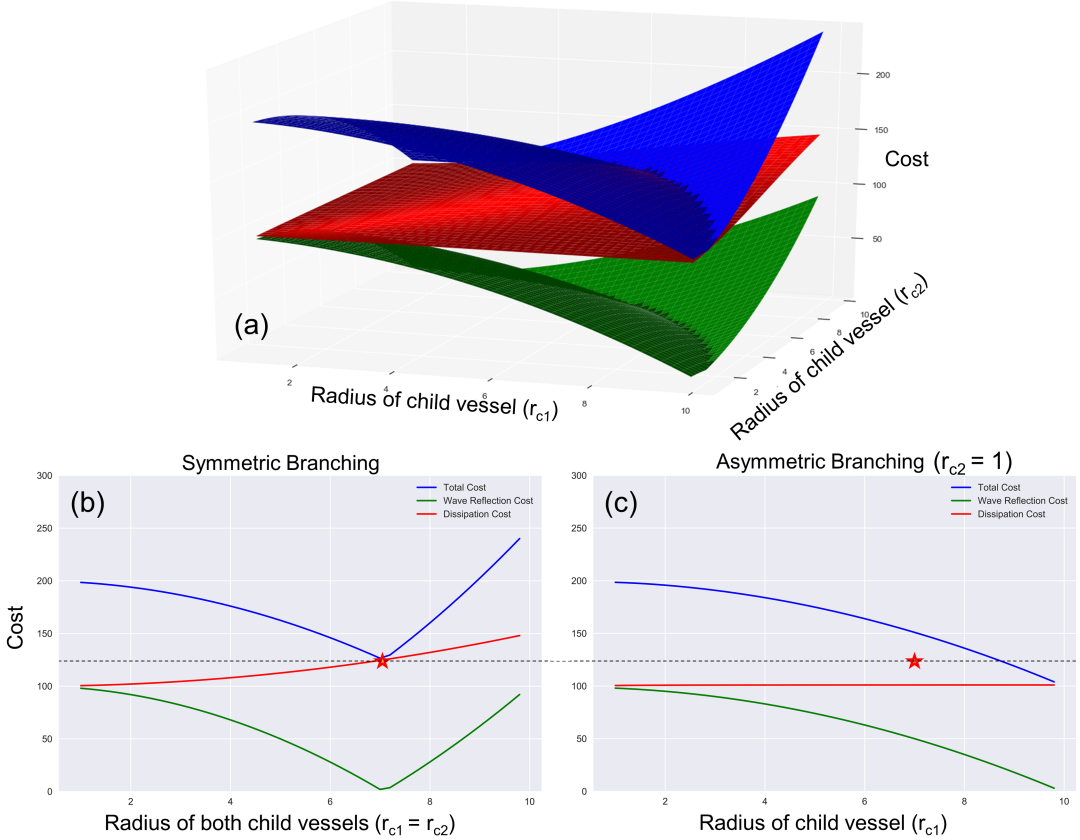


Figure 9: **Power loss minimization favors asymmetric branching.** (a) Depicts the cost surfaces of three metrics of energy loss: Wave reflection cost (green), energy dissipation cost (red) and a linear combination of the two (blue). (b) Depicts a projection of (a) on the diagonal plane, where symmetric branching occurs. (c) Depicts a projection of (a) on the  $r_{c2} = 1$  plane, that is when one of the vessels is very small. The minimum value of the total cost function in the symmetric case(b) is marked with a red star and projected to the graph of the asymmetric case(c).

As shown earlier, we have defined the cost due to power loss to be the combination of the cost due to wave reflections and the dissipation cost. In the case where only these two metrics are considered, the total cost of a network is identical to its cost due to power loss. In figure ?? we focus on a single branching point and examine the cost surfaces for wave reflections, dissipation and their combination. The minimum power loss cost value achieved in symmetric branching is found

to be higher than that achieved in the asymmetric case. As a result, we find that minimizing power loss as a combination of the cost due to wave reflections and dissipation should favor networks that branch highly asymmetrically.

As we add more terms to our cost function, the problem of optimizing networks becomes harder and harder for the algorithm to tackle. The increasing complexity of the task means that obtaining optimal structures for reasonably sized networks becomes very difficult and so we refrain from displaying direct renderings of network structure for higher order combinations. Instead, we focus on the scale factor distributions of the networks we generate as the effects of optimization become visible in that space even for sub-optimal networks.

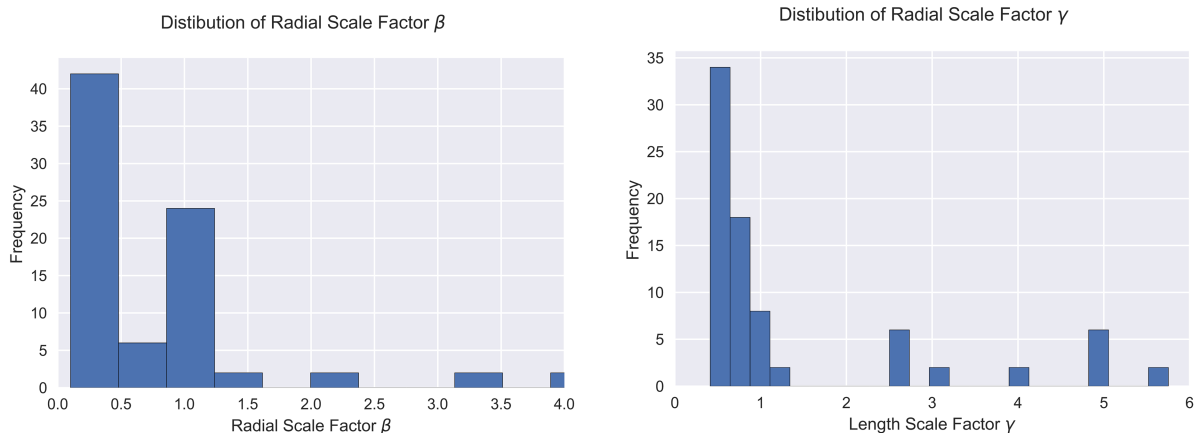


Figure 10: **Scale factor distributions for VVNs optimized for total path length and power loss.** The distribution of radial scale factors (left) is bi-modal with modes near 0 and 1 and mean value of 1.4. Bi-modality is a sign of high network asymmetry. The distribution of length scale factors (right) is long-tailed, a feature seen in all our generated networks.

The bi-modal distribution of the radial scale factor for networks optimized for total path length and power loss is consistent with our theoretical predictions. Total path length should have no direct effect on radii, as it is only a function of network length. However, its interaction with

the dissipation component of power loss should encourage vessel branching. The bi-modality in  $\beta$  distributions seems to be the result of the interaction of the two components of power loss, namely dissipation and wave reflections. The two metrics, as shown earlier, favor high network asymmetry and we interpret the two modes of the distribution as the signal of that asymmetry. A value of  $\beta$  near 0 is a result of a child vessel radius being much smaller than that of its parent. A value of  $\beta$  near 1 is a result of a parent and child vessel having near equal radii. The appearance of both values in the same family of networks seems therefore to be a signal of high network asymmetry. The distribution of length scale factors exhibits this long tailed shape which seems to be a product of optimizing for material cost in a space filling grid.

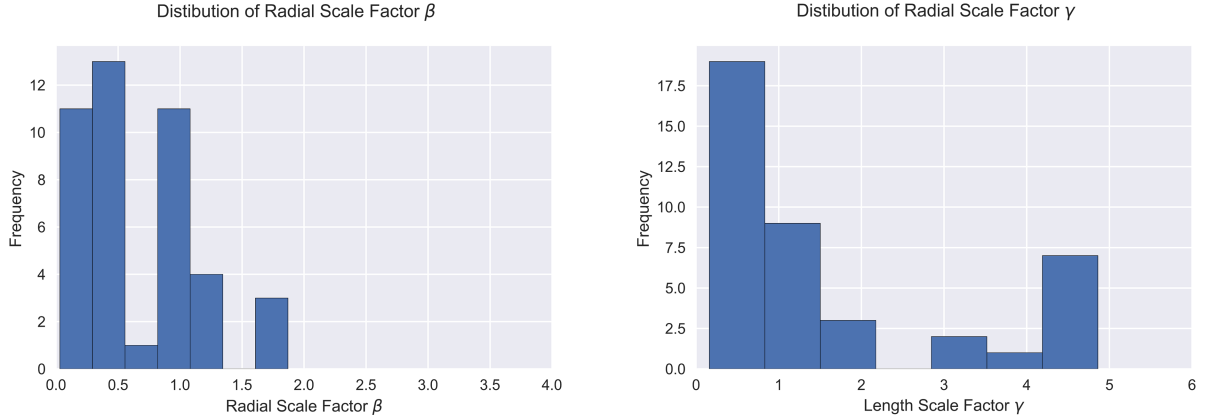


Figure 11: **Scale factor distributions for VVNs optimized for total path length, mean path length and wave reflections.** The distribution of radial scale factors (left) has a mean of 0.65. The distribution of length scale factors (right) is long-tailed.

The uni-modal distribution of  $\beta$  scale factors is more uniform than that of asymmetric networks and corresponds to a mix of symmetric and asymmetric branching. The interaction of total path length and mean path length should produce network connectivity similar to that of the networks examined earlier. The similar shape of the length scale factor distributions seems to support that.

Since wave reflections are the only power loss metric used for these networks, there is no selection pressure for asymmetric over symmetric branching and so a mix of the two is found in the networks.

### 4.3 Network Comparisons

In this section we present the scale factor distributions of mammal and plant networks and we compare them to our generated networks using a Welch's t-test. Because of the long-tailed shape of length scale factor distributions, we log-transform the  $\gamma$  values for all networks.

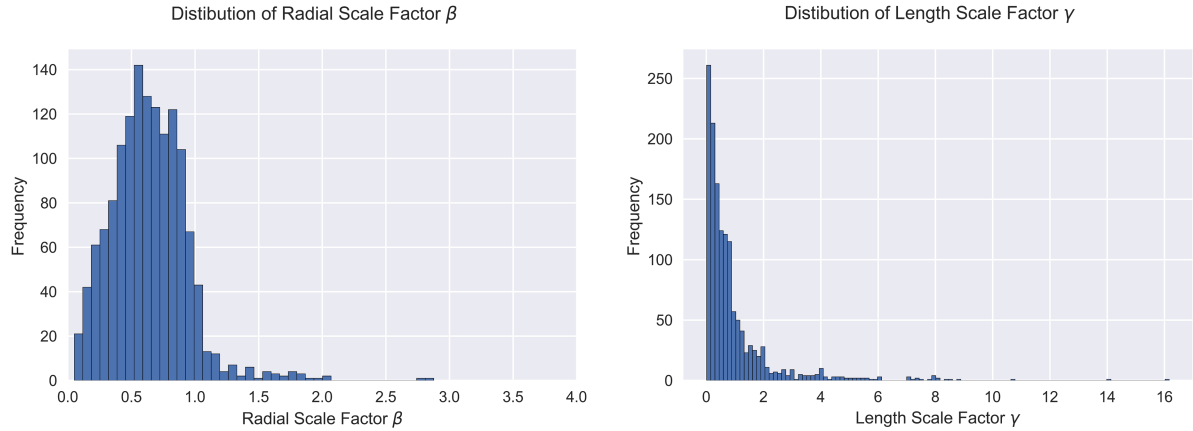


Figure 12: **Scale factor distributions for mammal networks.** The distribution of radial scale factors (left) has a mean of 0.82. The distribution of length scale factors (right) is long-tailed. Mammalian vascular networks tend to mostly branch symmetrically.

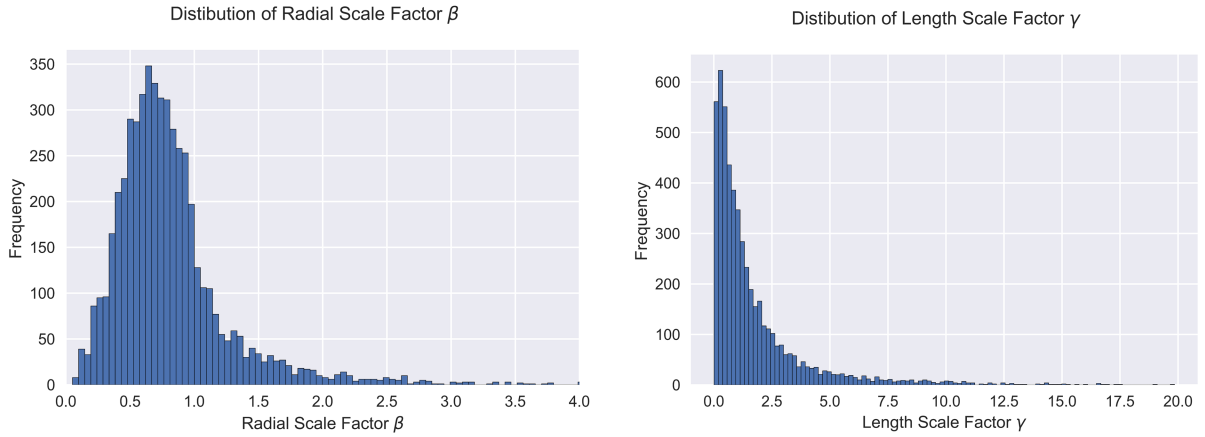


Figure 13: **Scale factor distributions for plant networks.** The distribution of radial scale factors (left) has a mean of 0.64. The distribution of length scale factors (right) is long-tailed. Plant networks tend to exhibit a mix of symmetric and asymmetric branching.

Optimization Criteria / Scale Factor	Radial Scale Factor	Log of Length Scale Factor
Total Path Length - Mean Path Length - Wave Reflections	0.034059116	0.771969776
Total Path Length - Dissipation - Wave Reflections	0.034782242	0.633701492

Table 1: **P-values for Welch's t-test between VVN<sub>s</sub> and Mammal networks.** With a significance level of  $\alpha = 0.05$ , two tests reject the null hypothesis that the distributions have the same mean.

Both families of generated networks exhibit a  $\beta$  distribution that is significantly different than that of the mammal networks. The  $\gamma$  distribution for both families of generated networks is not significantly different from that of the mammal networks.

Optimization Criteria / Scale Factor	Radial Scale Factor	Log of Length Scale Factor
Total Path Length - Mean Path Length - Wave Reflections	0.860905682	0.002044976
Total Path Length - Dissipation - Wave Reflections	0.006935715	0

Table 2: **P-values for Welch's t-test between VVNs and Plant networks.** With a significance level of  $\alpha = 0.05$ , all but one tests do not reject the null hypothesis that the distributions have the same mean.

Networks optimized for total path length and power-loss produced scale factor distributions that are significantly different than the plant distributions. Although networks optimizing total path length, mean path length and wave reflections had significantly different  $\gamma$  distribution compared to the plant networks, their  $\beta$  distribution was found not to be significantly different.

## 5 Discussion

Our virtual vascular network generator proved an effective tool for studying the forces that influence vascular structure. Expanding on previous work [9], our generator effectively optimizes networks for a variety of metrics by modeling their effects on both vessel radii and vessel lengths. Future work can aim to extend the generator’s functionality in a variety of ways. On one hand, the generator could be extended to consider more vascular network features such as vessel branching angles. Additionally, it would be possible to expand on the spacial architectures on which networks are developed to include other two dimensional spaces such as leaf shapes or three dimensional spaces such as spheres or realistic body plans. Finally, the generator could be generalized to simulate other types of biological structures such as neural networks.

Although there was some success reconstructing plant network radial scaling properties, our inability to reconstruct the mammal network  $\beta$  distribution (table 1) points to a missing component to our model. Particularly, it seems that the asymmetry produced by the interaction of power loss due to dissipation and power loss due to wave reflections (fig.9) is not a feature common in real networks. At the same time, the mix of symmetry and asymmetry seen in plant networks was replicated by VVN (table 2) that ignore the effects of power loss due to dissipation and optimize for mean path length instead (fig.11). We hypothesize that our model is missing at least one component that would favor symmetric over asymmetric branching. Such a component could match the effects of dissipation to produce mixed branching for plant networks and overpower dissipation to produce mostly symmetric networks in mammals. Possible constraints may include finite-size effects, due to which highly asymmetric branching would produce vessels too small to branch any further. Other possibilities include imposing a penalty for delivering “too much blood” to a network endpoint, as doing so to capillary vessels in a real network could result in tissue damage. Our work although fails to identify what this factor is, has provided a framework in the form of our VVN generator to test possible hypotheses.

The consistently long-tailed distribution of  $\gamma$  scale factors of VVNs is also an interesting result. While for some generated network families the length scaling distribution matches those of real networks (tab. 1), it contradicts the length scaling prediction of WBE theory. From our experience with the generator, it seems that the long-tailed length scaling distribution is the result of optimizing for total path length within our space-filling grid. As shown earlier, in the case where total path length alone is considered for optimization (fig.5), the problem reduces to finding the minimum spanning tree of all the points. Such a procedure can be solved using a greedy algorithm and the tendency to always prefer the smallest possible branch could give rise to the distributions like the ones observed.

Our work cannot definitively answer whether the modeling principles of WBE theory are sufficient to produce real networks. Although some aspects of real networks were recreated by our model, the comparisons between our VVNs and real data can be made more effective. Our use of the Welch's test proved not be ideal as some scale factor distributions deviated from the test's assumptions (fig. 10). Despite these limitations, in exploring our question we developed a robust framework in the form of our VVN generator that can form the basis of future work that both expands on ours and addresses novel question regarding biological networks.

## References

- [1] Knut Schmidt-Nielsen. *Scaling: why is animal size so important?* Cambridge Univ. Pr., 2012.
- [2] V. M. Savage, A. P. Allen, J. H. Brown, J. F. Gillooly, A. B. Herman, W. H. Woodruff, and G. B. West. Scaling of number, size, and metabolic rate of cells with body size in mammals. *Proceedings of the National Academy of Sciences*, 104(11):4718–4723, mar 2007.
- [3] Geoffrey B. West, James H. Brown, and Brian J. Enquist. A general model for the structure and allometry of plant vascular systems. *Nature*, 400(6745):664667, 1999.
- [4] G. B. West. The fourth dimension of life: Fractal geometry and allometric scaling of organisms. *Science*, 284(5420):16771679, 1999.
- [5] G. B. West. A general model for the origin of allometric scaling laws in biology. *Science*, 276(5309):122–126, apr 1997.
- [6] Alexander Byers Brummer, Van M. Savage, and Brian J. Enquist. A general model for metabolic scaling in self-similar asymmetric networks. *PLOS Computational Biology*, 13(3):e1005394, mar 2017.
- [7] Mitchell G Newberry, Daniel B Ennis, and Van M Savage. Testing foundations of biological scaling theory using automated measurements of vascular networks. *PLOS Computational Biology*, 11(8):e1004455, aug 2015.
- [8] Van M. Savage, Eric J. Deeds, and Walter Fontana. Sizing up allometric scaling theory. *PLoS Computational Biology*, 4(9):e1000171, sep 2008.
- [9] David Hunt and Van M. Savage. Asymmetries arising from the space-filling nature of vascular networks. *Physical Review E*, 93(6), jun 2016.
- [10] M. Welter, K. Bartha, and H. Rieger. Vascular remodelling of an arterio-venous blood vessel network during solid tumour growth. *Journal of Theoretical Biology*, 259(3):405–422, aug 2009.

- [11] Charles C. Palmer and Aaron Kershenbaum. Representing trees in genetic algorithms. In *Proceedings of the First IEEE Conference on Evolutionary Computation*, pages 379–384. IEEE Press, 1994.
- [12] Melanie Mitchell. *An Introduction to Genetic Algorithms*. MIT Press, 1998.
- [13] Alexander B Brummer, Panagiotis Lymeropoulos, Jocelyn Shen, Elif Tekin, Lisa P. Bentley, Vanessa Buzzard, Andrew Gray, Imma Oliveras, Brian J. Enquist, and Van M. Savage. Identifying branching principles in biological networks using imaging, modeling, and machine learning, 2019.
- [14] Peter B. Reich. The world-wide ‘fast-slow’ plant economics spectrum: a traits manifesto. *Journal of Ecology*, 102(2):275–301, feb 2014.
- [15] Mark E. Olson, Tommaso Anfodillo, Julieta A. Rosell, Giai Petit, Alan Crivellaro, Sandrine Isnard, Calixto León-Gómez, Leonardo O. Alvarado-Cárdenas, and Matiss Castorena. Universal hydraulics of the flowering plants: vessel diameter scales with stem length across angiosperm lineages, habits and climates. *Ecology Letters*, 17(8):988–997, may 2014.